

## Reconstruction of pure frequency sounds from glass vibration using a coupled Michelson-Fizeau interferometer

Name: Alie Craplet  
CID: 01335702

Supervisor: Dr Mark Scott  
Assessor: Professor David Colling

Word Count: 5996

## Abstract

This project presents a laser eavesdropping technique which uses a coupled Michelson-Fizeau interferometer to produce precise measurements of the amplitude and frequency of sound-driven glass vibrations. A Michelson interferometer is also used for cross-verification purposes. Multiple interferograms have been recorded with either an oscillating piezoelectric device or a microscope glass slice vibrating under pure frequency sounds. A comprehensive set of programs accurately reconstructing the amplitude and frequency of vibrations from the recorded interferograms has been written and tested. Simulation studies showed the strengths and limitations of each computational analysis process over the range of amplitudes and frequencies considered (from 2 to 10  $\mu\text{m}$  and from 20 to 60Hz). The amplitude (frequency) reconstructed from simulated data sets had an error of 10.5%(12%) for the Michelson interferometer technique and of 11%(1.5%) for the coupled interferometer technique. A frequency-independent linear relationship between the amplitude of movement of the piezoelectric stage and the input voltage was found, in line with theoretical expectations. The gradient of the line of best fit was found to be  $7.7 \pm 8 \times 10^{-5} \mu\text{mV}^{-1}$  and  $8.3 \pm 6 \times 10^{-4} \mu\text{mV}^{-1}$  with the Michelson and the coupled interferometer respectively. The frequency of vibration of a 0.57mm-thin glass slice driven by a sequence of pure frequency tones at a constant volume of  $68 \pm 5\text{dB}$  was accurately reconstructed. The average difference between the input and reconstructed frequency was 4.2% and the average error on the reconstructed frequency was 8.7%. The amplitude of oscillation was found to be  $0.93 \pm 0.3 \mu\text{m}$  which is consistent with the theoretical expectation of  $0.73 \mu\text{m}$ . Experimental factors account for 65% of the error and the limitations in the computational analysis make up the remaining 35%.

# Summary of Work Undertaken

The work on this project was split between my lab partner Aditya Sudharsanam and myself. The experimental work was likewise split between ourselves, and included devising the clamp design and setting up the experimental set-up. I wrote all analysis and simulation programs presented in this study. I also performed a large majority of the analysis of the interferograms over the course of the project. Aditya modelled the clamp on the software Solidworks and have written the code we used to convert and play the recorded sounds. He also wrote his analysis programs that I did not personally use. Neither of us had undertaken any summer placement or any prior work regarding this specific project.

This report is organised as follows. Section 2 presents the main theoretical aspect of this study, including a brief overview of the dynamics of vibrations in solids, an introduction to interferometry highlighting on the coupled Michelson-Fizeau interferometer and finally a presentation of piezoelectric devices and their remarkable properties. Section 3 summarises the experimental procedure followed in this study. Both two and three-waves experimental set-ups are presented, as well as the clamp that was designed and manufactured for the latter experiment. The algorithms written and used to extract the amplitude and frequency of motions in both the two and three waves interference cases are explained in Section 4. Section 5 presents and discusses the results of this investigation. It includes a study of the quality of the analysis procedures done using simulated interferograms. This section also presents a cross-verification of the two methods using the calibration of the piezoelectric stage. Finally, it also contains the reconstruction of frequency and amplitude of the sound-driven vibrations of a microscope glass slice in the case of pure frequency sounds. Section 6 gives a summary and a conclusion for this study, and includes some suggestions for further work.

# Contents

<b>1</b>	<b>Introduction</b>	<b>4</b>
<b>2</b>	<b>Theory</b>	<b>4</b>
2.1	Vibrations . . . . .	4
2.2	Interferometry . . . . .	5
2.2.1	Two-wave interference - Michelson interferometer . . . . .	5
2.2.2	Three-wave interference - Coupled interferometer . . . . .	6
2.3	Fourier transforms . . . . .	8
2.4	Piezoelectric devices . . . . .	9
<b>3</b>	<b>Experimental method</b>	<b>9</b>
3.1	Michelson interferometer with a piezoelectric actuator . . . . .	9
3.2	Michelson-Fizeau coupled interferometer . . . . .	10
<b>4</b>	<b>Computational analysis</b>	<b>12</b>
4.1	Analysis process for the Michelson interferometer . . . . .	12
4.2	Analysis process for the coupled interferogram . . . . .	14
<b>5</b>	<b>Results and discussion</b>	<b>17</b>
5.1	Verifying the quality of the analysis process against simulated data sets . . . .	17
5.1.1	Michelson interferometer . . . . .	17
5.1.2	Michelson-Fizeau coupled interferometer . . . . .	18
5.2	Calibration of the piezoelectric stage . . . . .	19
5.3	Testing with pure frequency sound . . . . .	21
<b>6</b>	<b>Conclusion</b>	<b>23</b>

# 1 Introduction

Interferometry is a very powerful experimental tool, among the most successful in 20<sup>th</sup> century Physics. Its applications cover a wide range of research areas, ranging from the search for gravitational waves [1] and astronomical observations [2] to the study of femtosecond-long radiation emissions in attosecond science [3]. This technique is also used outside of the research sphere for calibration in engineering [4], meteorology [5] and even for measuring small vibrations [6, 7].

This last application motivated this project with a simple question: is it possible to use light to eavesdrop on conversations via the precise measurement of a window vibration? It has been known for century that sound carries a certain amount of energy that causes the solids it encounters to vibrate [8]. If the vibrations of a reflective material can be accurately reconstructed from a distance using interferometry and if the relationship between the amplitude and frequency of the vibrations and the initial sound is known, then one can in theory eavesdrop on distant conversations using light. This spying method has already been used by the USSR around 1947 to try and spy on the French, Dutch and American embassies in Moscow[9]. The few available records and later attempts do not mention the use of interferometry for reconstructing the window vibrations but instead a measurement of the displacement of the laser beam reflected by the vibrating window [10, 11].

The experimental work presented here constitutes an investigation of the use of interferometry in the scope of laser eavesdropping. This project sets out to verify the hypothesis that small amplitude sound-driven vibrations can be accurately reconstructed via an interferometric study. With that scope in mind, a Michelson interferometer was assembled and a comprehensive set of programs has been written to extract measurements for the amplitude and frequency of motion from the recorded interferograms. The experimental set-up built for this study was found to be relatively efficient for simple sound reconstruction at a small distance from the source. There is also strong evidence showing that it can be adapted to the fields of medicine and engineering as it offers a precise and non-invasive means to measure small amplitudes and relatively high frequency vibrations.

## 2 Theory

### 2.1 Vibrations

Vibrations are omnipresent in our daily lives. The most common example is sound, defined as the propagation through a medium (often air) of an adiabatic compression or decompression [12]. Sound carries energy and upon contact with a solid, some of this energy is transferred to the object. The transferred energy can cause the solid to deform and/or oscillate back and forth about its equilibrium position [8]. For simplicity, let us consider the example of a circular plate of radius  $r_0$  vibrating under a uniform pressure  $P$ . The maximum amplitude of motion,  $w$ , of the plate is given by [13]:

$$w = 0.01142 \frac{P\pi r_0^2}{D} \tag{1}$$

where  $D$  is the flexural rigidity, defined as [14]:

$$D = \frac{Eh^3}{12(1 - \nu^2)} \quad (2)$$

where  $E$ ,  $h$  and  $\nu$  are the Young's modulus, the thickness and the Poisson ratio of the membrane respectively.

The load pressure  $P$  carried by a sound wave is measured in decibels by the sound's intensity  $L_p$ . The pressure and intensity are related as follows [15]:

$$P = 10^{L_p/20dB} P_0 \quad (3)$$

where  $P_0 = 20\mu\text{Pa}$  [15] is the reference pressure.

From equations (1) to (3) above, one can derive the amplitude of motion expected for a circular microscope glass slice of radius 2cm and thickness 0.57mm vibrating as a result of a typical loud conversation at 68dB [16]. Since Young's modulus for glass is 60GPa [12] and its Poisson ratio is 0.24[12], the theoretical amplitude of oscillation of this glass slice is  $0.73\mu\text{m}$ .

## 2.2 Interferometry

### 2.2.1 Two-wave interference - Michelson interferometer

Interferometry is the study of the interaction between two (or more) coherent waves [17]. In the first part of this study, the interference between coherent light beams is investigated using a Michelson interferometer similar to the one presented in Figure 1a) below.

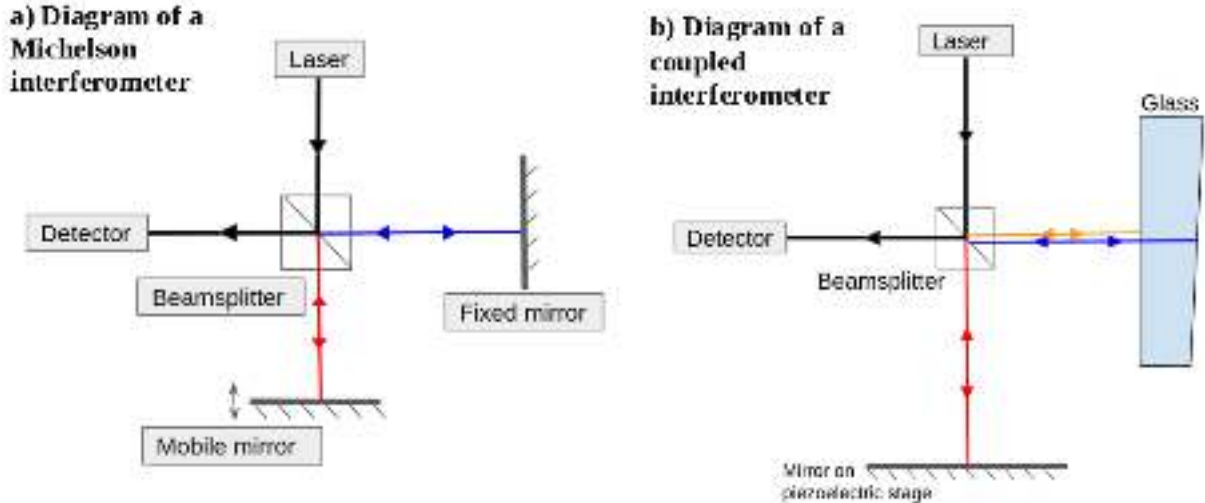


Figure 1: Diagrams of a Michelson interferometer (a) and a Michelson-Fizeau coupled interferometer (b). In the experiment presented here, one of the mirrors was mounted on a mobile piezoelectric actuator. The relative tilt between the two sides of the glass in b) is strongly exaggerated.

The difference in distance travelled by each beam,  $d_1 - d_2$ , gives rise to a phase difference  $\delta_1 - \delta_2$  between the two superimposed waves that results in an interference pattern upon recombination. The electric field corresponding to each separate wave travelling in the  $z$  direction has the following sinusoidal form [11]:

$$E_i = A \cos(kz - \omega t + \delta_i) \quad (4)$$

where  $k = \frac{2\pi}{\lambda}$  is the wave number of the light of wavelength  $\lambda$  and  $\omega = \frac{2\pi c}{\lambda}$  is the angular frequency of the light, with  $c$  is the speed of light and  $A$  is an arbitrary amplitude.

Upon recombination, the electric fields corresponding to both waves add up according to the principle of superposition [18]. The resultant wave has the following electric field:

$$E_{1,2} = E_1 + E_2 = 2A \cos\left(kz - \omega t + \frac{\delta_1 + \delta_2}{2}\right) \cos\left(\frac{\delta_1 - \delta_2}{2}\right) \quad (5)$$

The intensity recorded by a detector placed like that one in Figure 1a) is a function of the path difference between the two reflective surface since the intensity is proportional to the square of the electric field. Interferometry can therefore be used to measure small relative motions very accurately, as will be presented later.

### 2.2.2 Three-wave interference - Coupled interferometer

Figure 1b) presents an interferometer similar to the one used in the latter part of this study. In this interferometer, one of the mirror of the Michelson interferometer is replaced by a thin slice of glass. In this case the laser beam reflects off the two air-glass interfaces as well as off the mirror. This arrangement is referred to in literature [17] as a Michelson-Fizeau coupled interferometer. The glass wedge, if correctly aligned, acts as a Fizeau interferometer since the interference between the two reflected beams depends on the relative tilt between them.

The interference pattern for light reflecting off different surfaces and a perfect flat surface (that we take as one of the air-glass interfaces here) are reproduced from [19] in the Appendix (see Figure 21). A simulation of the interference pattern in the cases of almost and perfectly flat surfaces is shown in Figure 2a) and b).

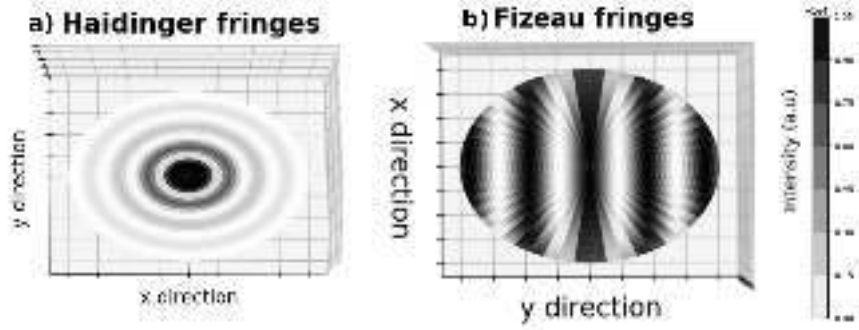


Figure 2: Simulation of the interference pattern that would be obtained from a) two parallel almost flat reflective surfaces and b) two perfectly flat reflective surfaces tilted with respect to one-another. The distance to the null point is arbitrarily chosen to qualitatively resemble the experimental results presented in Section 4.2

The interference pattern that is expected from a three-beam interferogram can be calculated as the superposition of the three interference patterns corresponding to the three possible two-beam combinations. From equation (5) describing two waves interference, and using the superposition principle, the total electric field is given:

$$\begin{aligned}
 E = \sum_{i < j, i=1}^3 E_{i,j} = & 2A \cos(\phi(z, t) + \bar{\delta}_{12}) \cos(\Delta_{12}) \\
 & + 2B \cos(\phi(z, t) + \bar{\delta}_{13}) \cos(\Delta_{13}) \\
 & + 2C \cos(\phi(z, t) + \bar{\delta}_{23}) \cos(\Delta_{23})
 \end{aligned} \tag{6}$$

where  $\bar{\delta}_{ij} = (\delta_i + \delta_j)/2$ ,  $\Delta_{ij} = (\delta_i - \delta_j)/2$ , and A, B and C are the respective strengths of each sub-interference and  $\phi(z, t) = kz - \omega t$  is common to all waves.

Applying equation (6) to the coupled interferogram described above with a slightly curved mirror and two perfectly flat glass surfaces, slightly tilted with respect to one-another gives the interference pattern presented in Figure 3. Since glass has a reflection coefficient of 4% [12], the two beams reflecting at the air-glass interfaces are less intense than the beam reflecting from the mirror (which has a reflectivity of 1). This difference in intensity between the interference pattern is taken into account in equation (6) by the A, B and C coefficients and is also accounted for in the simulation presented in Figure 3.



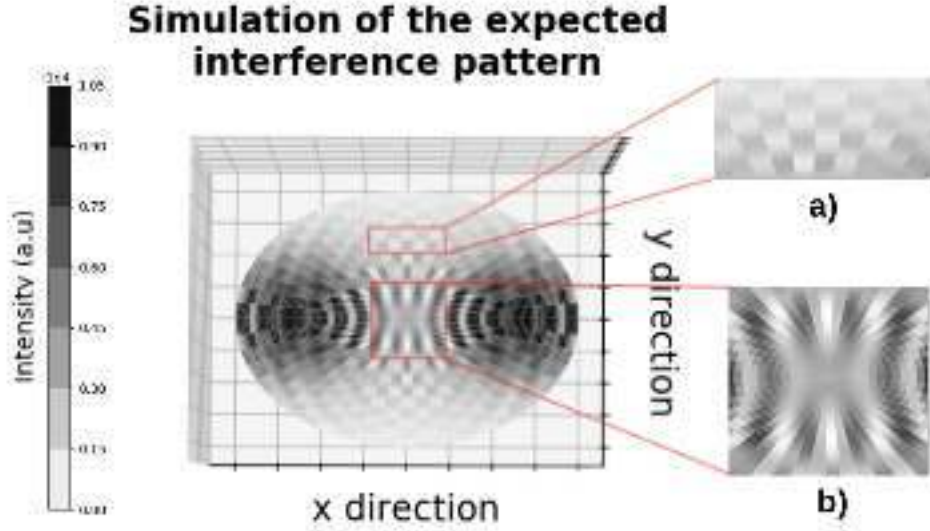


Figure 3: Simulation of the interference pattern that would be obtained from a three-beam interference between a thin slab of glass and a mirror. The relative distances to null point and angle of tilt were arbitrarily chosen to imitate the experimental values. The inserts present b) the central region of the pattern, when the mirror is close to parallel to the glass surfaces and a) when the mirror is significantly tilted with respect to the glass slice.

The simulation results shown in Figure 3 show a large difference with the interference pattern shown in Figure 2a), expected from a simple Michelson interferometer. This more complicated pattern is more sensitive to small misalignment and small motions [19], like for example, sound-driven vibrations in the glass slice.

## 2.3 Fourier transforms

A Fourier transform decomposes any time-dependant signal into the weighted sum of the pure frequency periodic signals that compose it [20]. In particular, if the signal is periodic then the Fourier transform is a finite sum of discrete waves. The Fourier transform  $g(\omega)$  in the frequency domain ( $\omega$ ) of a function  $f(t)$  in the time domain ( $t$ ) is given by [21]:

$$g(\omega) = \mathcal{F}[f(t)] = \frac{1}{\sqrt{2\pi}} \int_{-\infty}^{+\infty} f(t) e^{i\omega t} dt \quad (7)$$

and reciprocally,

$$f(t) = \mathcal{F}^{-1}[g(\omega)] = \frac{1}{\sqrt{2\pi}} \int_{-\infty}^{+\infty} g(\omega) e^{-i\omega t} d\omega \quad (8)$$

For experimentally collected data, the function  $f(t)$  is discrete, composed of a finite number of points, collected at a frequency  $f_{\text{samp}}$ , i.e. the sampling frequency of the measuring device used.

In the case presented here, the measured intensity of light depends on the position of both reflectors, as per equation (6). If the position of the reflector varies at a given frequency, as in the case for vibrations described in 2.1, then a Fourier transform reflects the frequency of oscillation [20].

## 2.4 Piezoelectric devices

For some materials a change in their shape induces a modification of their macroscopic electrical polarisation [22]. Conversely, they can be deformed by the appliance of an electric potential across them. These materials are called piezoelectric sensors and actuators, including for example lead-zirconate-titanates (PZT) ceramics [23] or quartz ( $\text{SiO}_2$ ) [22].

To increase the efficiency of conversion of electrical to mechanical energy, multiple layers of piezoelectric materials can be stacked into a Piezoelectric Stack Actuator (PSA) thus increasing the total range of motion of the device [22]. The relationship between the longitudinal deformation  $\Delta L$  of a PSA and its voltage input  $V$  is as follows [24]:

$$\Delta L = nd_{33}V \quad (9)$$

where  $n$  is the number of stacked layers of dielectrics and  $d_{33}$  is a proportionality constant. Piezoelectric devices can therefore easily be used as calibration devices provided the proportionality coefficient is known.

## 3 Experimental method

### 3.1 Michelson interferometer with a piezoelectric actuator

The first set-up used was a Michelson interferometer similar to the one shown in Figure 1a). A green laser beam of wavelength 533nm is directed towards a beamsplitter and separated into two beams of equal intensity. These beams reflect upon two heavily damped mirrors - where one mirror is mounted on a PSA piezoelectric actuator controlled by a variable voltage input - and then interfere upon recombination. The resulting interference pattern is recorded by a silicon photo-detector. A picture of the set-up is presented in Figure 4.

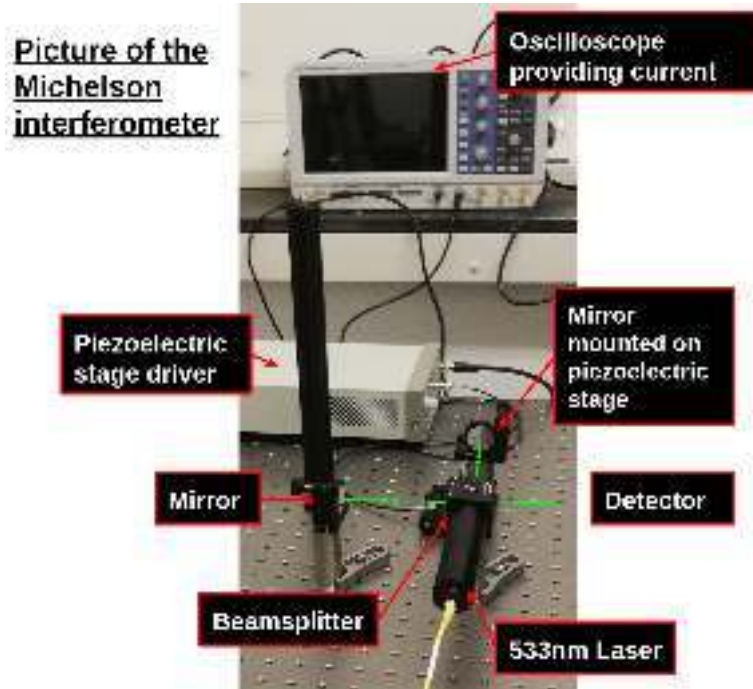


Figure 4: Picture of the Michelson interferometer used in the first half of this project. The green lines indicate the direction of the laser beams.

As seen in Section 2.4 the distance travelled by the piezoelectric stage is proportional to the instantaneous voltage it receives. The mirror mounted on the piezoelectric stage is used to model a surface vibrating under the effect of a sound. This is done by powering the actuator with a sinusoidal current. The fragile nature of the piezoelectric device and the instrumental limitation in the current's peak to peak amplitude and frequency lead to a restriction of the range of investigated frequencies between 0.1 and 50Hz.

### 3.2 Michelson-Fizeau coupled interferometer

A coupled Michelson-Fizeau interferometer like the one presented in Figure 1b) was then used to measure the effect of sound. A mount that would both support the glass slice and allow it to vibrate had to be designed and manufactured. The model of the designed clamp is shown in Figure 5a),b). A picture of the printed clamp holding a thin steel sheet is shown in Figure 5c).

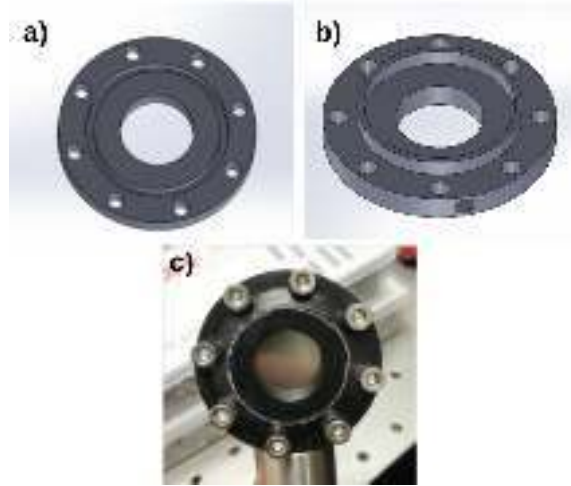


Figure 5: Design of the clamp top a) and bottom b) parts showing the 8 screw holes as well as the supplementary fixing hole to mount the clamp onto a standard optical support. Picture credit, Aditya Sudharsanam. The picture of the 3D printed clamp in c) shows how the clamp is assembled to hold a thin stainless steel sheet.

Figure 6 shows the coupled Michelson-Fizeau interferogram used in the second part of this study including the 0.57mm-thin slab of glass mounted on the designed clamp and a speaker for sound production. The speaker was fixed above the optical table and right behind the slab of glass. This prevented any propagation of vibrations through the table and ensured that the distance between the glass and speaker was kept constant. The CCD camera shown in Figure 6 was exchanged for a silicon photo-detector to perform time-resolved measurements.

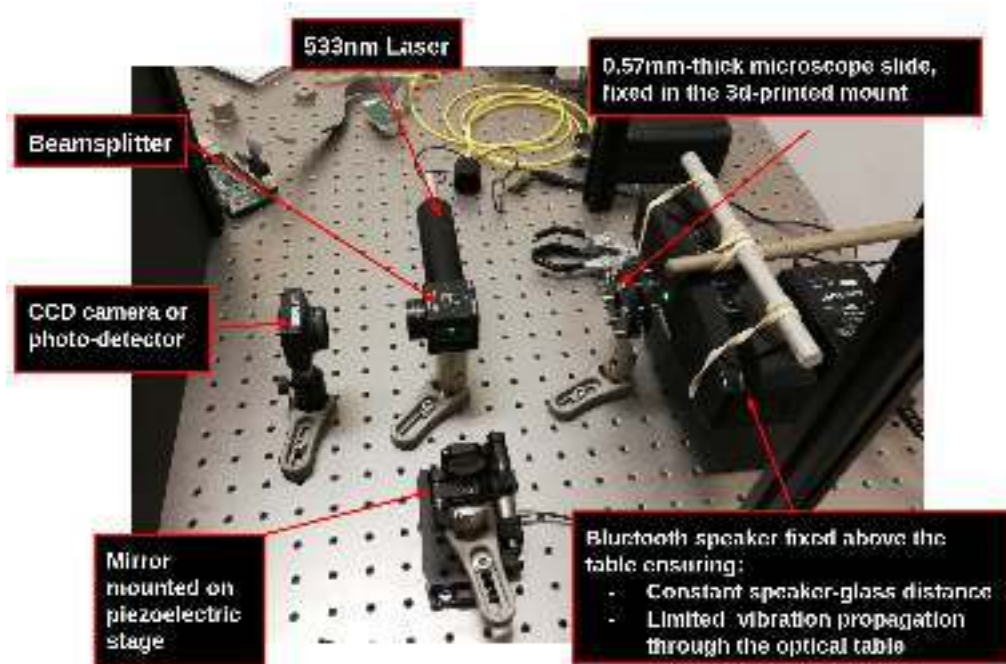


Figure 6: Picture of the coupled interferometer used in this study. The speaker is used to play extracts of melodies, conversations and pure-frequency tones at variable volumes.

## 4 Computational analysis

### 4.1 Analysis process for the Michelson interferometer

A short video of the time-varying interference pattern recorded with the Michelson set-up is available online at [https://www.youtube.com/watch?v=ty5J3m74R\\_E](https://www.youtube.com/watch?v=ty5J3m74R_E). Closer inspection of this video reveals how the oscillation of the mirror modifies the interference pattern. As the mirror moves forward a certain number of wavelengths, the corresponding number of bright and dark fringes are crossed in the interference pattern, as expected from equation (5). The mirror then slows down and reverses direction before crossing the same amount of fringes backwards, if the amplitude of oscillation is constant. The intensity of a small portion of this interferogram is recorded and shown in Figure 7(top).

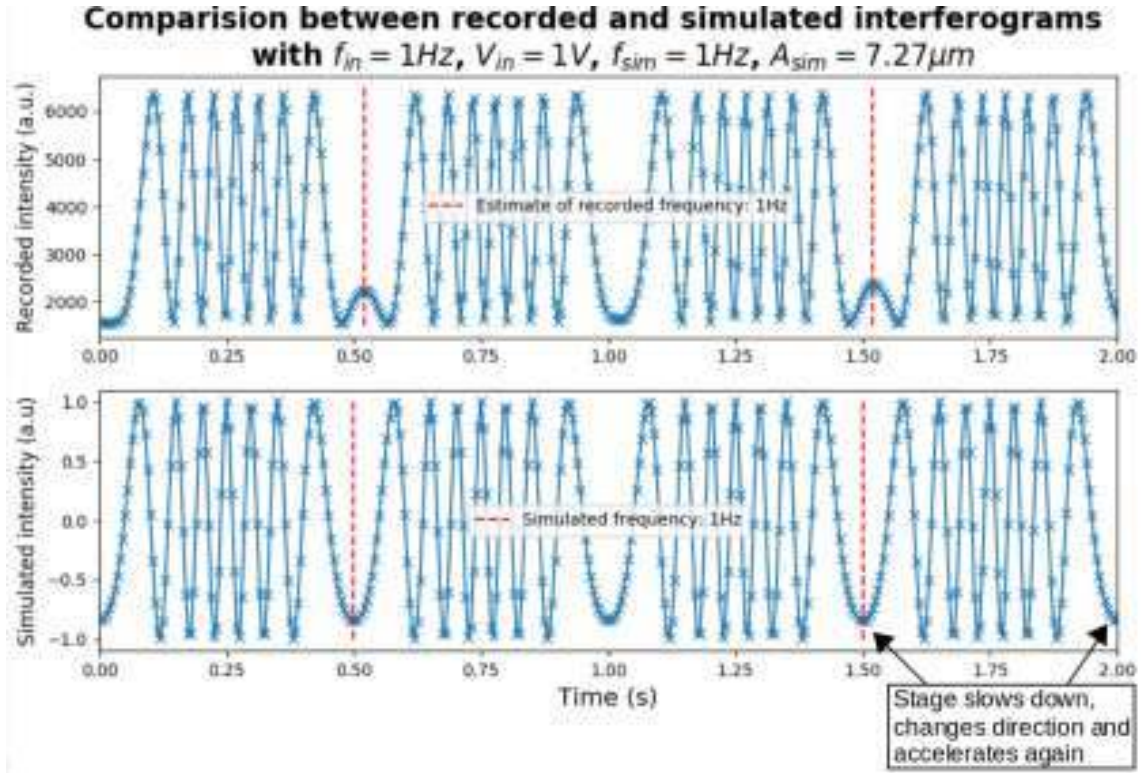


Figure 7: Qualitative comparison between the interferogram recorded with the piezoelectric stage oscillating under a sinusoidal input voltage of 1V peak-to-peak with frequency of 1Hz (top) and the simulation of a similar situation with a mirror oscillating over a distance  $A_{sim}=7.27\mu m$  at the same frequency (bottom).

It is interesting to compare the recorded interferogram presented in Figure 7(top) with a simulated interferogram. The simulation produces the interference pattern corresponding to a known amplitude and frequency of oscillation as per equation (5). The simulated interferogram for the stage oscillating at a frequency  $f_{sim}=1\text{Hz}$  and an amplitude  $A_{sim}=7.27\mu m$  is shown in Figure 7(bottom).

The interferograms can be analysed to retrieve the amplitude and frequency of motion of the moving mirror. For the Michelson interferometer, this analysis relies on measuring the



stage's velocity. As shown in Figure 8(top), the difference in intensity,  $|\Delta I|$ , oscillates between a maximum value and zero back and forth about the equilibrium position, just like the stage's velocity. A small  $\Delta I$  corresponds to the stage moving slowly as it reverses direction and a large positive (negative)  $\Delta I$  corresponds to the stage moving towards a bright (dark) fringe, where the two beams are in (anti-)phase.

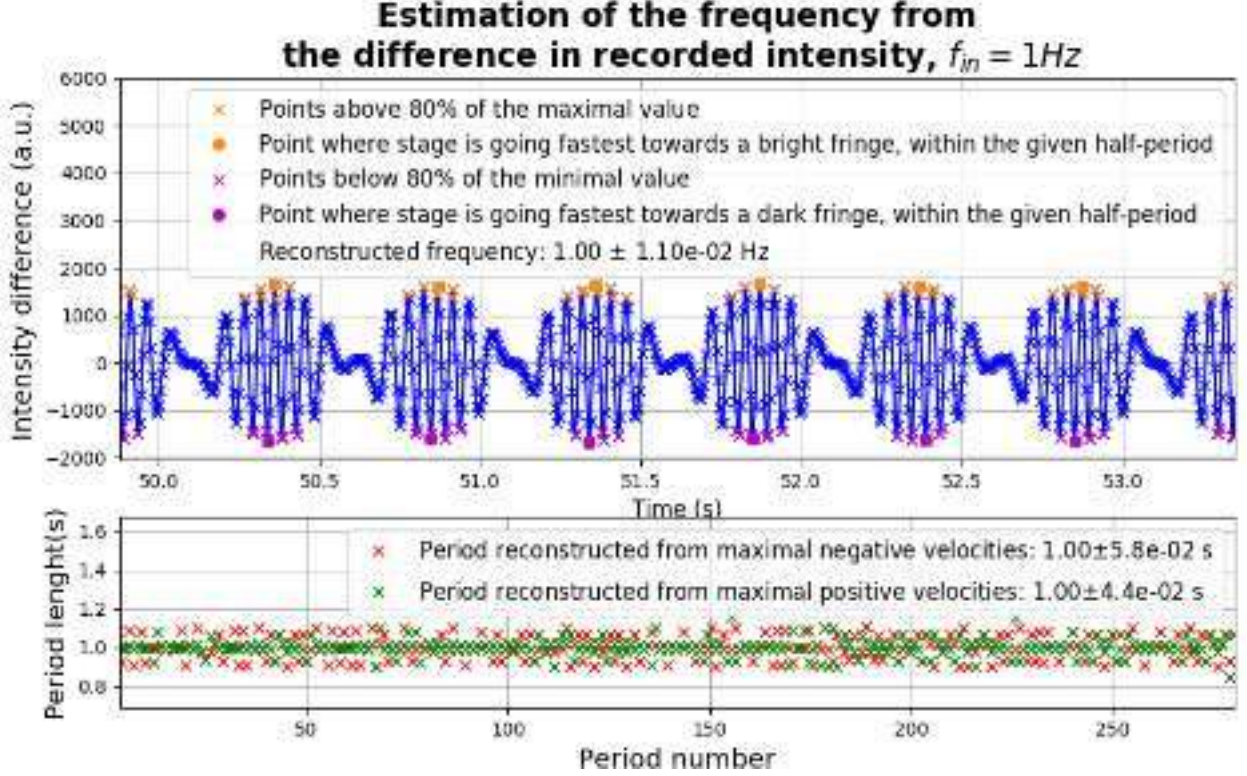


Figure 8: Diagram presenting the method used to analyse the recorded interferogram based on the difference in intensity between consecutive points. With the piezoelectric stage oscillating under a current of voltage  $V_{in} = 1V$  and frequency  $f_{in} = 1Hz$ , the reconstructed frequency is  $1.00 \pm 0.01Hz$

From time-stamps at which maximum and zero velocity occur, a period, and therefore a frequency, can be obtained for the signal as shown in Figure 8 (bottom). Since the frequency of oscillation is expected to be constant, an average can be done over the frequency estimate found for each oscillation. This helps lower the overall error on reconstruction.

Once the frequency is measured, the amplitude of motion can be estimated. From equation (5), the distance travelled by the stage between two consecutive bright fringes is known to be one wavelength of the laser light, i.e.  $\lambda = 533nm$ . From this, the difference in intensity can be linked to the distance travelled by the stage via the simple relation:

$$d = \frac{|\Delta I|}{2I_{pp}} \lambda \quad (10)$$

where  $d$  is the distance travelled between two consecutive points, and  $I_{pp}$  is the peak to peak intensity of the interferogram, corresponding to the difference in intensity between a dark and

a bright fringe. The piezoelectric stage has to be displaced by distance much larger than  $\lambda$  prior to any investigation to ensure that the calibration value  $I_{pp}$  was correct. Equation (10) was applied to one-period portions of the interferogram to give the average distance traveled over one period and a standard deviation across all the periods.

## 4.2 Analysis process for the coupled interferogram

Pictures of the interference patterns obtained with the coupled interferometer are shown in Figure 9. They are consistent with the expectations presented in Figure 3 and confirm at least qualitatively the hypothesis of three-wave interference.

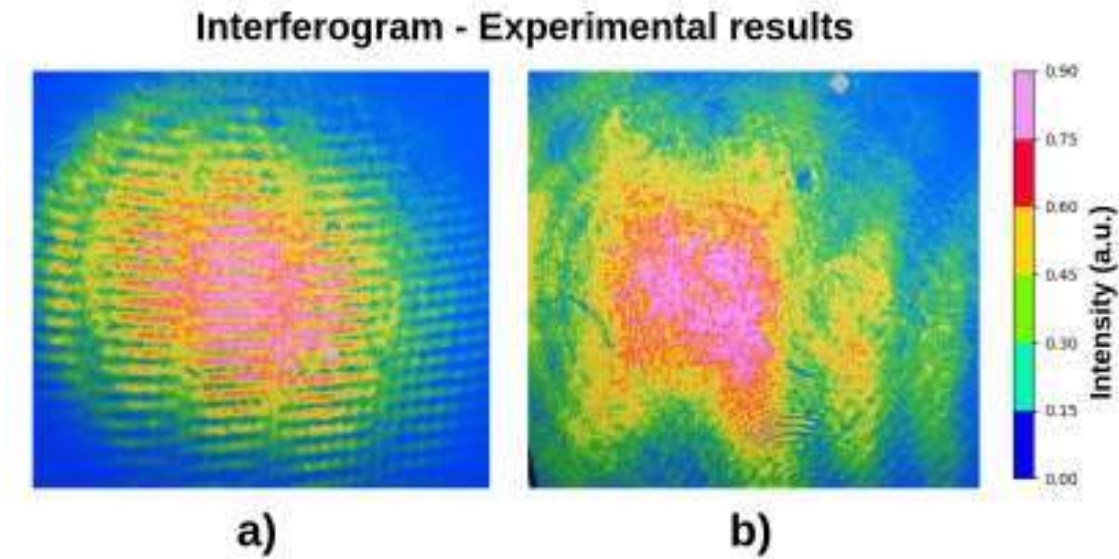


Figure 9: CCD picture of the observed interferogram a) when the mirror on the piezoelectric stage is not aligned and b) when it is in aligned optimally. It should be mentioned that the light is dimmed differently in cases a) and b) to ensure high resolution and prevent saturation.

The interference pattern corresponding to the reflection only on both sides of the glass is presented in Figure 10. This pattern presents wide and straight fringes which can be linked to the interference between flat and slightly tilted surface as explained in Section 2.2.2 and in Appendix.

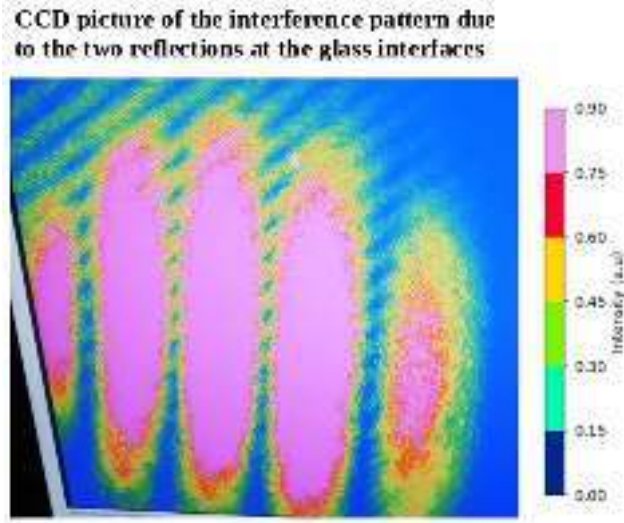


Figure 10: CCD picture of the interference pattern recorded when the mirror is covered and only the light reflecting from the two glass-air surfaces is interfering. The thin and faint interference fringes on the top left corner, thought to be caused by a small misalignment inside of the beamsplitter.

The preliminary results shown in Figures 9 and 10 confirm that the experimental results are consistent with the theoretical model of the coupled interferometer presented previously. Because the interference pattern in this case is very different from the one recorded with a Michelson interferogram, a different analysis process was required.

The shape of the interferogram was found to depend on at least five independent parameters: the instantaneous position of both the mirror and the glass slice, the thickness and refractive index of the glass slice and the relative tilt between the slice's two interfaces with air. A simulation of the interference pattern depending on all of these parameters and following equation (6) was written and then fitted to the experimental data using the package *Iminuit*. A first value of the frequency was determined using a Fourier transform of the signal. An example is presented in Figure 11, where the frequency is estimated from the separation of consecutive harmonics peaks in the frequency domain. Providing the fitting algorithm with this initial estimate of the frequency and restricting the allowed frequencies to a  $\pm 5$  sigma range around this initial guess greatly improved the fitting accuracy.



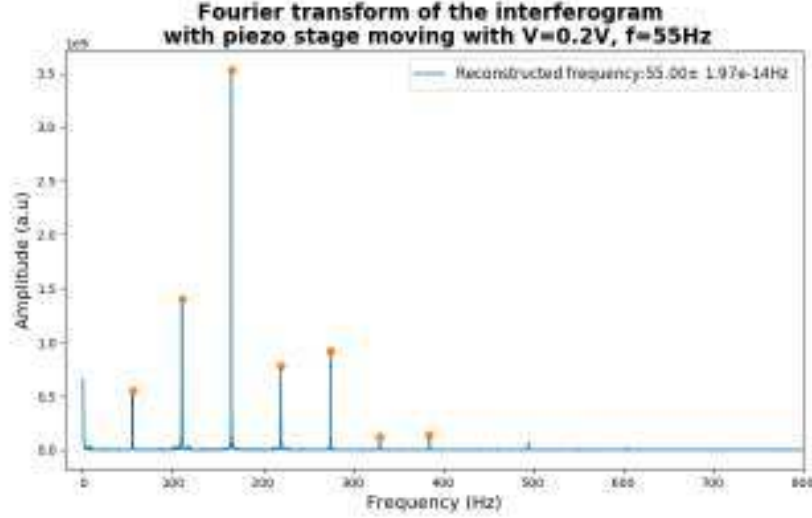


Figure 11: Fourier transform of the interferogram recorded when the piezoelectric stage was driven at 55Hz. The observed peaks in the frequency domain correspond to the harmonics present in the signal. The frequency estimation and the associated error are performed by measuring the separation in frequency between consecutive peaks and taking the standard deviation of the set.

The fit was performed in small batches of data corresponding to two or three periods as determined by the Fourier analysis which was performed on the complete data set. Weighted averages of the fitted amplitude and frequency were then performed over the whole region, ignoring the portions of data over which the fit failed. Figure 12 presents a case where the fitting process succeeded.

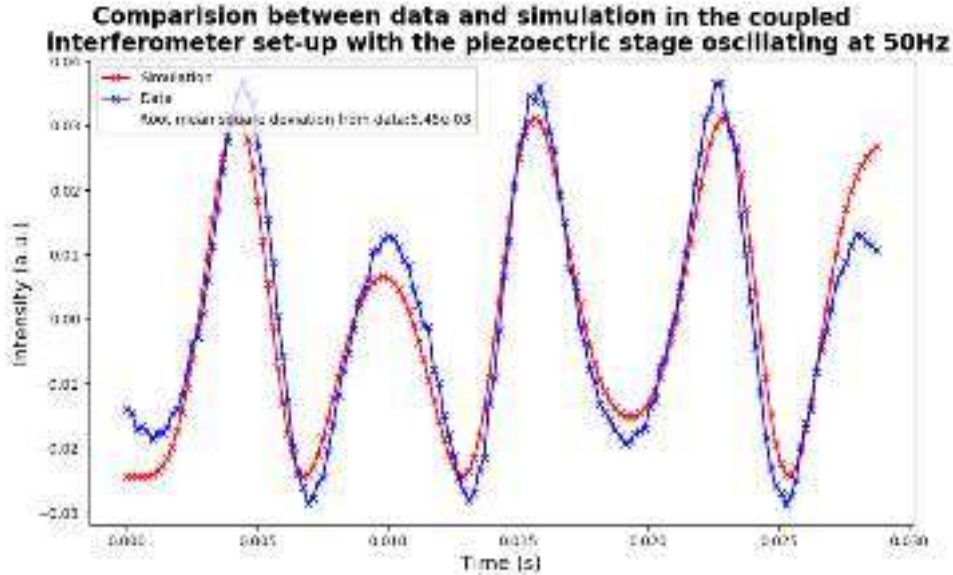


Figure 12: Interferograms recorded (blue) and simulated (red) corresponding to the piezoelectric stage oscillating at 50Hz under a 0.9V in the coupled interferogram set-up. This figure shows the analysis for a single period.

The number of points fitted together was optimised in order to reduce the average error

on the fit. Some constraints on the fitting parameters were also implemented to prevent any non-physical results. The quality of the fit was determined by calculating the average relative distance between the simulation and the data. The error on the fit  $\sigma$  was calculated as follows:

$$\sigma = \frac{1}{N} \sum_{i=1}^N \left( \frac{|r_i - s_i|}{r_i} \right) \quad (11)$$

where  $N$  is the total number of point and  $r_i$  and  $s_i$  are respectively the recorded and simulated intensities of the  $i^{th}$  point.

## 5 Results and discussion

### 5.1 Verifying the quality of the analysis process against simulated data sets

#### 5.1.1 Michelson interferometer

Before performing any tests with real data, the reconstruction programs have to be tested against simulated data sets to verify their accuracy and find their limitations. The results of this investigation in the Michelson interferometer case are shown in Figure 13. This figure presents the ratio of the difference between the input and reconstructed frequency (left) amplitude (right) over the relevant input values.

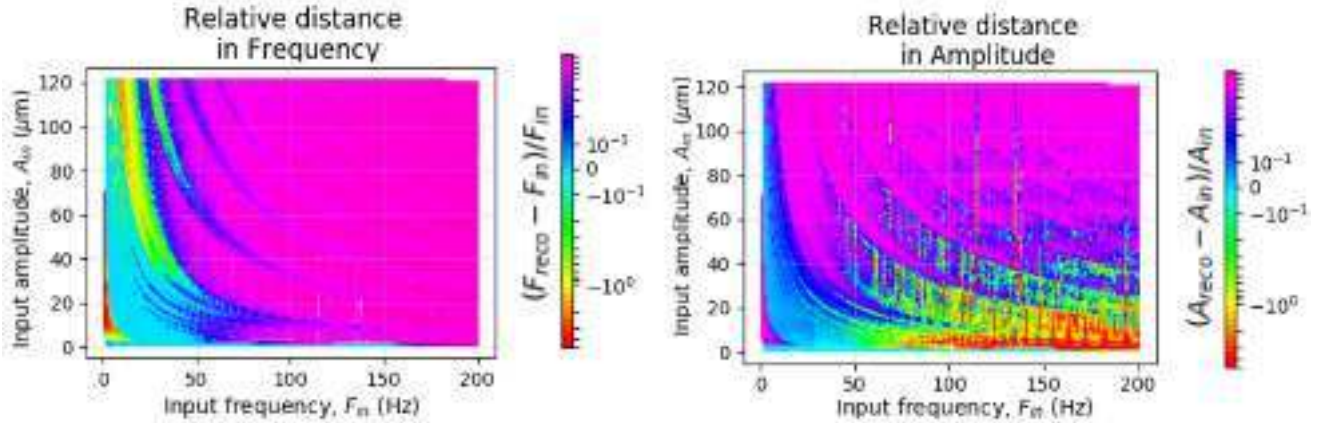


Figure 13: Relative distance between the simulated and reconstructed frequencies (left) and amplitude (right) as a function of the input frequency and amplitude. The analysis process, if successful for low amplitude and low frequencies is less accurate at high amplitudes and frequencies. All the simulations have been constructed with a sampling frequency of 6 211Hz, corresponding to experimental limitations.

As shown in Figure13 the Michelson interferometer reconstruction program is mostly accurate for input frequencies between 0 and 50Hz and for amplitude of motions between 0.5 and 20  $\mu\text{m}$ . In this range, the average difference between the input and reconstructed amplitude (frequency) is 7.1% (0.2%) of the input value. The non-zero lower bound in amplitude for the range over which the fitting is efficient is due to the fact that oscillations of amplitude

below the laser wavelength (533nm) cannot be properly reconstructed as mentioned in Section 4.1. This investigation confirms that the analysis technique can be used with confidence on interferograms corresponding to stage oscillations of low frequency and amplitudes.

Figure14 presents the relative error on the reconstruction of the amplitude and frequency, calculated as the ratio of the standard deviation on the reconstructed values over the input values.

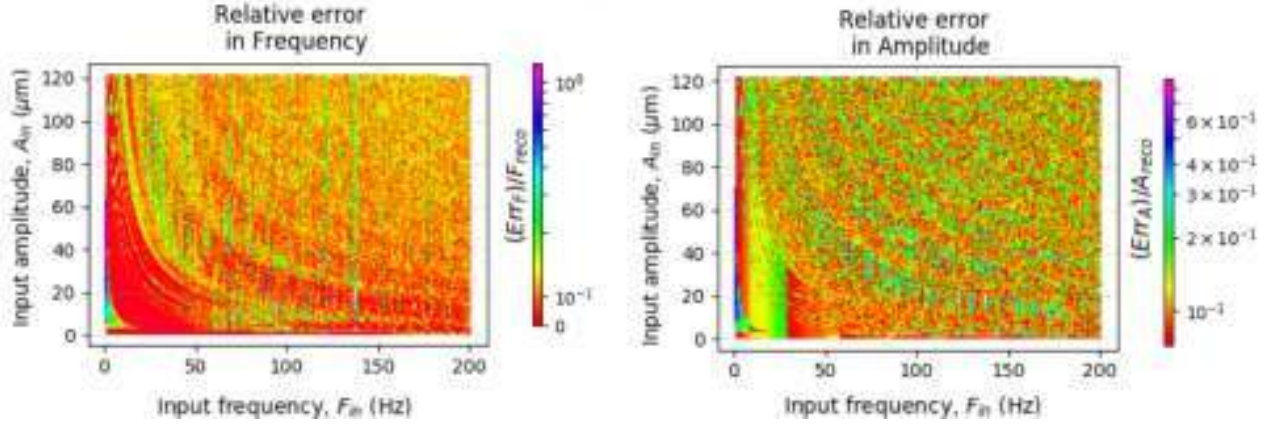


Figure 14: Fractional error on the reconstruction of the frequency (left) and amplitudes (right) of four seconds-long simulated Michelson interferograms.

The error on the reconstructed amplitudes and frequencies oscillates between 2% and 30%. Over the range of amplitudes and frequencies mentioned previously, the average error on the amplitude (frequency) is 10.5% (12%). At frequencies and amplitudes below 10Hz and 30 $\mu$ m the error is high with values about 40%, showing the limitations of the fitting process.

### 5.1.2 Michelson-Fizeau coupled interferometer

The same analysis was done for the coupled interferogram. The difference between the input of the simulation and the reconstructed amplitude is shown in Figure 15 alongside the associated error. The program is both precise and accurate in the reconstruction of the low amplitudes of motion. The error on the reconstruction is independent of the input values and has an average value of 11%.

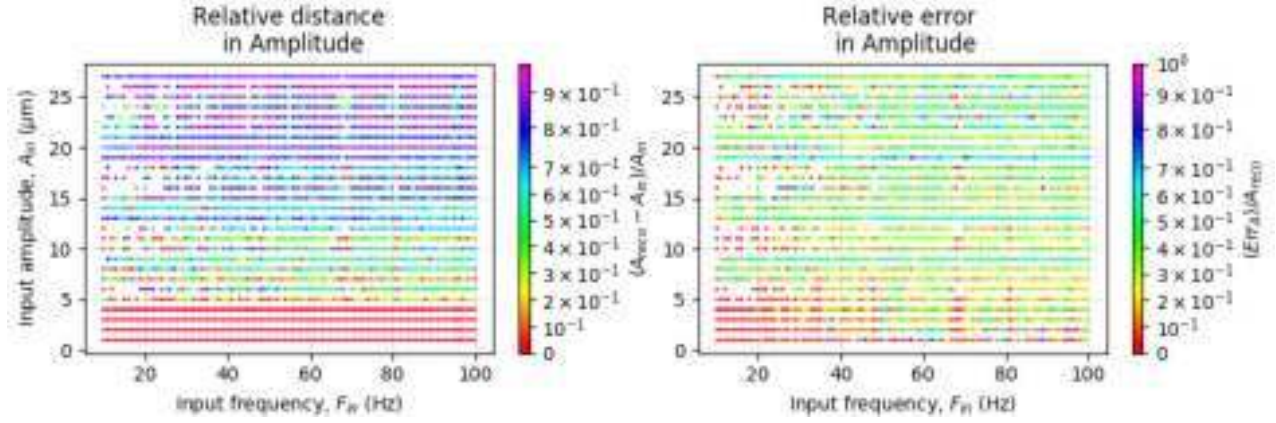


Figure 15: Amplitude reconstructed (left) and the associated error (right) from four seconds-long simulated interferograms in the coupled interferometer case.

The same analysis for the frequency is presented in Figure 16.

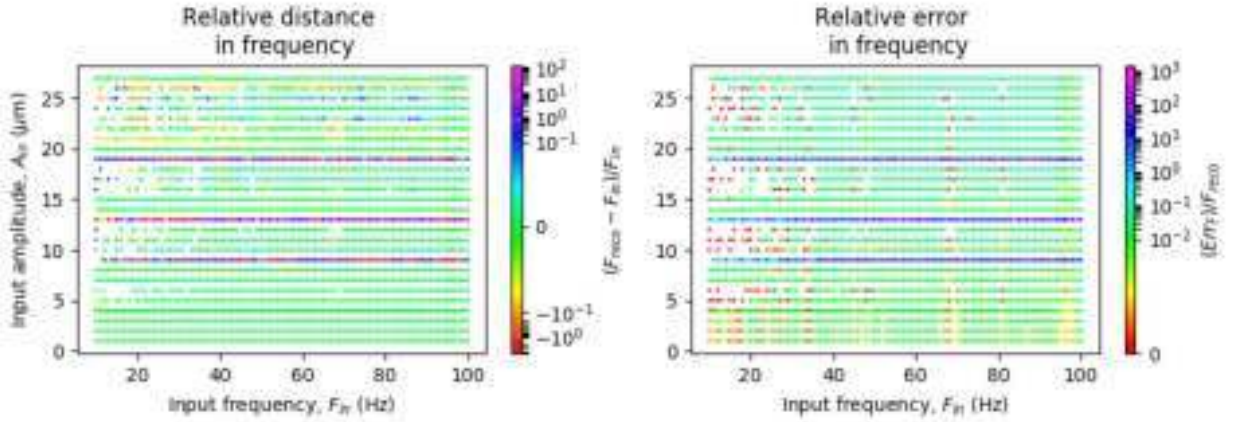


Figure 16: Frequency reconstructed (left) and its associated error (right) obtained from the analysis of four seconds-long simulated interferograms.

The reconstruction of the frequency presented in Figure 16 indicates that the frequency is reconstructed with a high precision and a low level of error except at certain amplitudes, namely 9, 13 and 19  $\mu\text{m}$ . Further investigations are however required to determine precisely the cause of the fitting failures observed at these amplitudes.

## 5.2 Calibration of the piezoelectric stage

The analysis method described in Section 4.1 was used on interferograms recorded using the Michelson interferometer with the piezoelectric stage oscillating under a sinusoidal input current of different frequency and voltage. The reconstructed amplitude as a function of the input voltage is shown in Figure 17. On this figure, the amplitude of motion of the stage is seen to be linearly dependent on the input voltage with a gradient  $7.7 \mu\text{mV}^{-1}$ . This relationship is independent of the frequency of the current and consistent with the theory of piezoelectric



devices as depicted in equation (9).

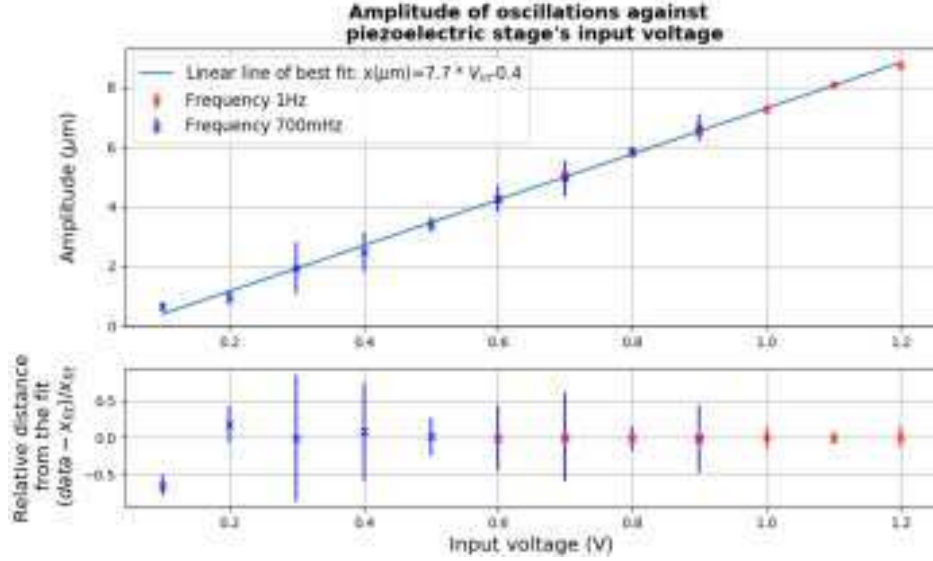


Figure 17: Value of the reconstructed amplitude as a function of the input voltage at two different input frequencies: 700mHz (red) and 1Hz (blue). The linear line of best fit to the data is shown (top) and the relative distance to the line of best fit is presented for each point (bottom).

The amplitude of oscillation reconstructed using the Michelson interferogram was then compared to the one reconstructed using the coupled Michelson-Fizeau interferometer to verify the agreement between the two analysis techniques. The results are presented in Figure 18.

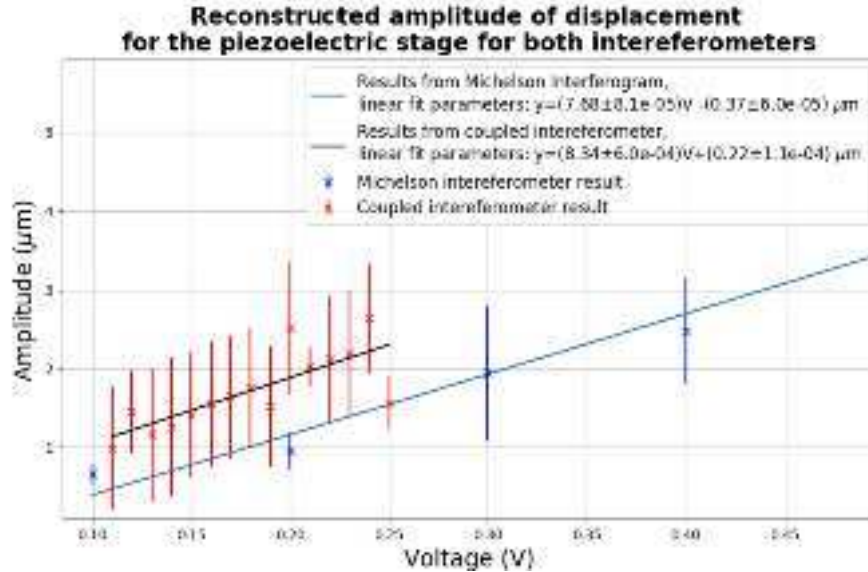


Figure 18: Comparison between the amplitude of motion for the piezoelectric stage reconstructed with the Michelson and the coupled interferometer as well as their respective linear line of best fit. The equation and error associated to each parameter of the line of best fit are presented in the legend.

Figure 18 shows that the piezoelectric stage’s amplitude of motion retrieved with either method is linearly dependant on the input voltage. The parameters of the linear fit  $y = \text{gradient} \times V_{in} + \text{intercept}$  are given in Table 1 below.

Method	Gradient ( $\mu\text{mV}^{-1}$ )	Intercept ( $\mu\text{m}$ )
Michelson interferometer	$7.68 \pm 8 \times 10^{-5}$	$-0.3 \pm 6 \times 10^{-5}$
Coupled interferometer	$8.34 \pm 6 \times 10^{-4}$	$0.2 \pm 1 \times 10^{-4}$

Table 1: Parameters of the linear line of best fit linking the amplitude of motion of the piezoelectric stage to its input voltage as retrieved by each method. The difference in intercept can be explained by the difference in analysis techniques. The error on each fit parameter is given from the covariance matrix of the fit.

The two fit presented in Table 1 present different values for both parameters of the linear fit. The error on the gradient and intercept is higher in the coupled interferogram case compared to the Michelson one, with values 7.4 and 1.8 times higher respectively. These differences can be explained by the differences in the reconstruction algorithms. A direct fitting of the interferogram, as in the case of the coupled interferogram is expected to be more accurate but with a larger error. This is because the number of points fitted together is invariant and function of the frequency which is very accurately determined by the Fourier transform. Conversely, the amplitude estimation done when reconstructing the amplitude in the Michelson case is based on measuring the amplitude over many period. This second method is repeated more more than the first giving a lower error of the reconstruted values.

### 5.3 Testing with pure frequency sound

The set-up and analysis technique described above were then tested with pure-frequency sound produced by the speaker at constant volume and directed towards the glass slice, which vibrated in response. A simple song was used for testing. The corresponding interference pattern can be seen on the video available on Youtube at <https://youtu.be/XedpwNeVKio>. In this video the impact of the glass vibrations on the interference pattern is clearly seen both when the glass and mirror are well aligned and when they not. The interferogram corresponding to a similar investigation is shown in Figure 19. The song is composed of five consecutive tones at 35, 45, 55, 45 and 35Hz respectively. Each of these tones lasts for 1 second and a pause of 0.3 seconds is observed in-between each tone. The results of the analysis of the recorded interference pattern are shown in Fig 20.

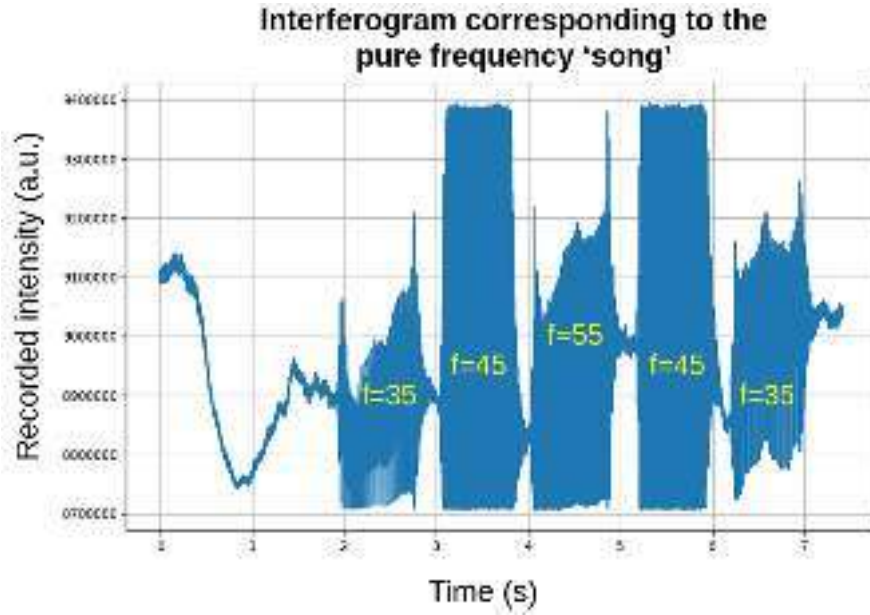


Figure 19: Interferogram recorded when the glass was vibrating under a song composed of 1 second segments of pure frequency between 35 and 55Hz.

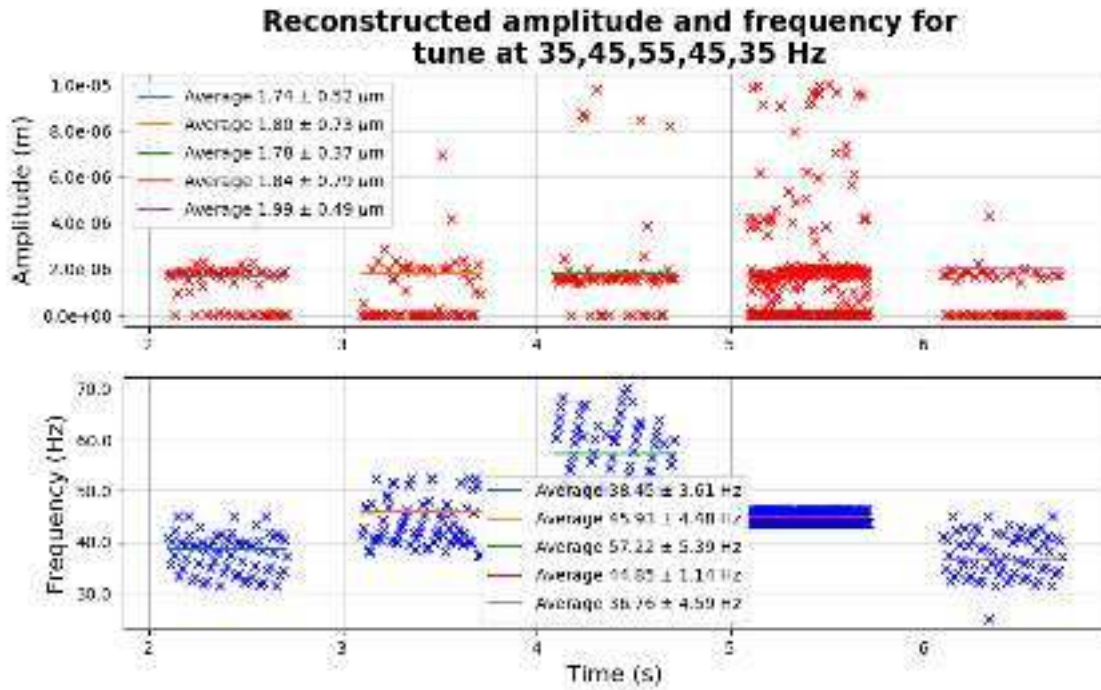


Figure 20: Results of the analysis of the interferogram recorded when the glass slice was vibrating under the song showing the amplitude and frequency reconstructed for each portion of the signal as well as the standard deviation on each measurement.

Figure 20 indicates that the program is quite efficient at extracting the frequency of sound with an error on the frequency varying between 2.5% and 12.5% of the reconstructed value

with an average error of 8.7%. The average distance between the driving and reconstructed frequency is 4.2% of the driving frequency. In every case, the driving frequency is contained within the margin of error of the reconstructed one.

The amplitude of oscillation of the glass over a full period is almost constant with an average value of  $1.83\mu\text{m}$  and an average error of 31.7% which corresponds to a peak to peak amplitude of  $0.93\pm 0.3\mu\text{m}$ . This value is coherent with the theoretical expectation of  $0.73\mu\text{m}$  presented in Section 2.1 which corresponds to a loud conversation. The theoretical value is contained within the margin of error. This result should however be taken with caution, as the volume of the sound fluctuated between 63dB and 73dB over the course of the data taking, mostly due to poor instrumental quality.

The sources of error present in this experiment are both experimental and due to the limitations in the analysis program. They are summarised in Table 2 alongside their estimated magnitudes.

Source or error	Estimated amplitude (Fractional contribution to error)
Loudspeaker inconsistencies	$\pm 5\text{dB}$ (plus cracking noises) ( $\sim 50\%$ )
Computational limitations	11.5% of the reconstructed amplitude (35%)
Elastic stress in glass	Estimated significant from interference pattern outline ( $\sim 15\%$ )
Interference within the beamsplitter	$\pm 15\%$ in recorded intensity (Negligible, it is a constant position-dependant offset)
Shear motion in glass	Negligible when alignment is correct [25]
Misalignment of the mirrors	Negligible (Accounted for in the fitting process)

Table 2: Main sources of error and their contribution to the error on the reconstructed amplitude. The values are experimentally measured where possible and compared with the literature otherwise.

Table 2 summarises the different sources of error and their contribution to the total error on the amplitude reconstruction. The experimental statistical errors, dominated by the loudspeaker deficiencies and the time-delay and elastic stress within the glass slab account for approximately 65% of the total error. The systematical limitations of the analysis process represent 35% of the total error when working at low frequencies and amplitudes.

## 6 Conclusion

This study presented two analysis programs that permitted the reconstruction of the amplitude and frequencies of oscillations of reflective surfaces for a Michelson interferometer and a coupled Michelson-Fizeau interferometer. The accuracy of each program has been tested against simulated interferograms showing error levels on amplitude (frequency) of 10.5%(12%)



and 11%(1.5%) for the Michelson and coupled interferometers respectively.

The amplitude of motion of a piezoelectric stage was reconstructed with both methods and found to be linearly dependant on the input voltage and independent of the frequency of motion in accordance with the theoretical expectations. The linear fit to the data sets had values of  $y_{\text{Michelson}}(\text{in } \mu\text{m}) = (7.68 \pm 8 \times 10^{-5})V - (0.3 \pm 6 \times 10^{-5})$  and  $y_{\text{Coupled}}(\text{in } \mu\text{m}) = (8.34 \pm 6 \times 10^{-4})V + (0.22 \pm 1 \times 10^{-4})$  for the Michelson and coupled interferograms respectively. The two values are consistent and the discrepancies between the two can be explained by the different analysis procedures.

Finally, the motion of a thin glass vibration under pure frequency tones was measured using the interferometric method presented. The frequency of the incoming sounds was reconstructed with an error of 8.5% and an average distance to the sound frequency of 4.2%. The peak to peak amplitude of oscillation, expected constant was reconstructed as  $0.93 \pm 0.3 \mu\text{m}$  which is consistent with the theoretical expectation of  $0.73 \mu\text{m}$  for a similar glass slab vibrating under a 68dB pure frequency sound.

The technique presented in this study was found to be very efficient at reconstructed low-frequencies tones at typical speech volumes. However, when tested with speech recordings it was found to be inefficient, mostly because speech frequency varies too rapidly. Currently, this technique does not present a large improvement on laser eavesdropping techniques already available. It is, however, a very robust and non-intrusive method for small periodic motion measurement and could easily be adapted to precise vibration or fine motion measurements in the fields of medicine or engineering.

## Acknowledgements

I would like to thank all the people that made this investigation possible. My deepest thanks go to Graham Axtell, Ivan Hermida and Lee Parker for their invaluable help and advice. I also would like to acknowledge the technical help provided to us by Johan Borg. His help has proven to be critical to the success of this investigation. I would also like to thank Dr. Mark Scott and Prof. David Colling for their precious insight throughout this project. Finally, I could not write this report without thanking my project partner Aditya Sudharsanam without whom nothing would have been possible.

# Appendix
















Surface type	Appearance of the Newton fringes	
	Without tilt	With tilt
Plane		
Almost plane		
Spherical		
Conical		
Cylindrical		
Astigmatic (curvatures of same sign)		
Astigmatic (curvatures of opposite sign)		
Highly irregular		

Figure 21: Table presenting the aspect of the interference patterns for different types of surfaces with and without a tilt relative to the reference mirror. Adapted from [19].

# References

- [1] Abbott BP, Abbott R, Abbott TD, Abernathy MR, Acernese F, Ackley K, et al. GW151226: Observation of Gravitational Waves from a 22-Solar-Mass Binary Black Hole Coalescence. *Physical review letters*. 2016;116(24):241103.
- [2] Fowler JW, Doriese WB, Marriage TA, Tran HT, Aboobaker AM, Dumont C, et al. Cosmic microwave background observations with a compact heterogeneous 150 ghz interferometer in chile. *The Astrophysical Journal Supplement Series*. 2005;156(1):1–11.
- [3] Usenko S, Przystawik A, Jakob MA, Lazzarino LL, Brenner G, Toleikis S, et al. Attosecond interferometry with self-amplified spontaneous emission of a free-electron laser. *Nature Communications*. 2017;8(1).
- [4] Sun Q, Wang JI, Hu HB. A primary standard for low- g shock calibration by laser interferometry. *Measurement Science and Technology*. 2014;25(7):075003.
- [5] Yang D, Buckley SM. Estimating High-Resolution Atmospheric Phase Screens From Radar Interferometry Data. *IEEE Transactions on Geoscience and Remote Sensing*. 2011;49(8):3117–3128.
- [6] Solís SM, Santoyo FM, Hernández-Montes MDS. 3D displacement measurements of the tympanic membrane with digital holographic interferometry. *Optics express*. 2012;20(5):5613.
- [7] Koyuncu B. Semi-automatic measurements of small high-frequency vibrations using time averaged electronic speckle pattern interferometry. *Journal of Physics E: Scientific Instruments*. 1980;13(2):206–208.
- [8] Rossing TD. *Principles of vibration and sound*. New York: Springer-Verlag; 1994.
- [9] Nikitin P. Leon Theremin (Lev Termen). *IEEE Antennas and Propagation Magazine*. 2012;54(5):252–257.
- [10] Solomon J, Prigo R. Eavesdropping with a laser. *American Journal of Physics*. 1987;55(4):381–381.
- [11] Yan-Hong F, Ye L, Xiao-Feng M, Jing-Sai J, Qiu-Yun H, Ya-Chen W. Research on Anti-Laser-Eavesdropping Devices. In: *2012 International Conference on Industrial Control and Electronics Engineering*. IEEE; 2012. p. 1981–1983.
- [12] Fahy F. *Sound and structural vibration : radiation, transmission and response*. 2nd ed. Amsterdam ; London: Elsevier/Academic; 2007.
- [13] Ventsel E, Krauthammer T, Carrera E. *Thin Plates and Shells: Theory, Analysis, and Applications*. *Applied Mechanics Reviews*. 2002;55(4):B72–B73.
- [14] Nagaya K, Nagai K. Dynamic response of circular plates in contact with a fluid subjected to general dynamic pressures on a fluid surface. *Journal of Sound and Vibration*. 1986;106(2):333–345.

- [15] SS/7. BS EN 60027-3:2007 - Letter symbols to be used in electrical technology. Logarithmic and related quantities, and their units; 2008.
- [16] Brimicombe M. Safe and sound: measuring decibels electronically. Project Diary: sound level meter. Electronics Education. 2004;2004(3):10–17.
- [17] Totzeck M. Interferometry. In: Springer Handbook of Lasers and Optics. Berlin, Heidelberg: Springer Berlin Heidelberg; 2012. p. 1255–1283.
- [18] Bermúdez de Castro Aa. Mathematical Models and Numerical Simulation in Electromagnetism; 2014.
- [19] Optical shop testing. Hoboken, N.J.: Wiley-Interscience; 2007.
- [20] Smith a Winthrop W. Handbook of real-time fast Fourier transforms : algorithms to product testing; 2015.
- [21] James JFJF. A student’s guide to Fourier transforms with applications in physics and engineering. Cambridge: Cambridge University Press; 2011.
- [22] Rupitsch SJa. Piezoelectric Sensors and Actuators Fundamentals and Applications; 2019.
- [23] Khalid M, Shoaib M, Khan AA. Strontium doped Lead Zirconate Titanate ceramics: Study of calcination and sintering process to improve piezo effect. Journal of Nanoscience and Nanotechnology. 2011;11(6):5440–5445.
- [24] ThorLabs. Operational Theory of Piezoelectric Stacked Actuators;. Available from: [https://www.thorlabs.com/newgrouppage9.cfm?objectgroup\\_id=5030](https://www.thorlabs.com/newgrouppage9.cfm?objectgroup_id=5030).
- [25] Engineering Fundamentals. Displacement of a clamped circular plate under a uniformly distributed load;. Available from: [https://www.efunda.com/formulae/solid\\_mechanics/plates/calculators/cpC\\_PUniform.cfm](https://www.efunda.com/formulae/solid_mechanics/plates/calculators/cpC_PUniform.cfm).